UWB Channel Characterization for Compact L-Shape Configurations for Body-Centric Positioning Applications

Richa Bharadwaj, *Member, IEEE,* Srijittra Swaisaenyakorn, Clive Parini, *Member, IEEE,* J. C. Batchelor, *Member, IEEE* Shiban K. Koul, *Fellow, IEEE* and Akram Alomainy, *Senior Member IEEE*

***Abstract*— This paper presents an analysis on the body-centric channel parameters classification for various compact 3 base station L-Shape configurations utilizing only a 2D-plane for installation. Four different L-Shape configurations (*x-z*/*y-z plane*) are studied (facing-front/side/back) by varying the position of the base stations in an indoor environment. Results and analyses highlight the variation of the channel parameters with respect to the orientation of the base station configurations and presence of the human subject. Channel parameters values (peak power delay profile (PDP)/rms delay spread /Kurtosis) are reported for (line of sight (LOS): -65 to -50 dB/0.5-5 nsec/40-60) and (non-line of sight (NLOS): -80 to -65 dB/ 10-25 nsec/ 5-25). The 3D localisation accuracy obtained is highest (1-3 cm) for the *x-z plane* L-Shape configuration facing-front which has maximum number of LOS links (70 %).The accuracy decreases by 1-2 cm for the *x-z plane* L-Shape configuration facing-back due to increase in NLOS links (70 %) between the wearable antennas and the base stations.**

***Index Terms*— Ultra-Wideband (UWB), Channel Characterization, Positioning, Body Area Networks**

I. Introduction

The evolving need of compact and user-friendly localization and tracking devices has paved a way for new research areas and market opportunities in the body area networks (BAN) domain [1-2]. Among various wireless technologies present such as Bluetooth, Wi-Fi, UWB and ZigBee, UWB is the most suitable technology for high accuracy (mm to cm range) localisation [2-4]. UWB technology offers attractive features such as high data rate communication, fine time resolution, low power, low cost, compact antenna design, integration with other technologies and ease of implementation which is very suitable for bodycentric communication [4-6].

Several UWB based localization systems such as Ubisense, Eliko, BeSpoon, DecaWave, Time Domain PulsON, Open RTLS, Pozyx, have accuracy of 10–15 cm [3,5]. For achieving 3D localisation a minimum of four base stations (BSs) while applying trilateration/triangulation based on angle of arrival (AOA), received signal strength (RSS), time of arrival (TOA) and time difference of arrival (TDOA) algorithms [2-3,7]. Works have been carried out using four or more base stations to obtain high cm accuracy of the target in various domains such as patient tracking for healthcare applications [8], robotics [9], asset tracking [5], monitoring sportsmen [10], indoor motion gaming [11] and localisation of the human subjects [3, 12-14]. Various state-of-the art techniques such as ray tracing [9], kalman and extended finite impulse response filter [12-13], integrated UWB and inertial tracking [12], propagation path information [15], array antenna [16] for localization is reported in open literature.

In the presence of more than four BSs, the high NLOS links (leading to inaccurate range estimation) can be ignored or weighted localization algorithms can be applied to enhance accuracy [13,15]. But for various applications that demand high tracking accuracy and the use of less number of BSs, channel classification methods and NLOS mitigation techniques need to be applied. In our previous work, four or more BSs have been used for 3D human body localisation using channel information and time of arrival (TOA) based algorithms [3, 14]. For applications that have more space constraints and still aim for very high tracking accuracy, more compact, scalable, and easily portable BSs configurations need to be looked into.

This paper presents a compact 2D plane L-shape configuration placed in various orientations in the localization domain and an in depth channel analysis to mitigate NLOS effects to increase the localization accuracy. The L-Shape configuration leads to reduction in occupancy volume by using a 2D plane configuration instead of commonly used 3D BS configurations such as Cuboid-Shape configuration. Section II describes the measurement setup, proposed BSs configurations in four different orientations for body centric localisation and the localisation algorithm. The results are analyzed and discussed in Section III related to the channel characteristics for the different wearable sensor locations and BS links and the localisation accuracy achieved. Section IV presents the conclusion with the important findings and contributions.

II. Measurement Setup

Body-centric localisation measurements were performed in a motion capture studio lab. The wearable antennas were placed on the joints of the arms/legs and the torso region over a 3×3 grid to study the propagation channel type and localisation results.

The human subject is standing at the center of the localisation area of 1.8 × 1.8 m^2 and has average built and height of 168 cm. The 3BSs are positioned near the vertices of the cuboid in an L-Shape configuration with BS1 as the reference co-ordinate at (0,0,0) (Fig. 1. (a)). The schematic of the L-shape configuration set up is presented in Fig. 1(b).

Compact and low cost tapered slot co-planar waveguide fed UWB tapered slot antennas (TSA) with dimensions of 27 mm × 16 mm were used as the body-worn sensor and the BSs. The TSA antenna offers better than 10 dB return loss with good radiation performance and relatively constant gain across the UWB spectrum [4]. VICON motion capture system [3] was used as reference providing standard 3D positioning data with an accuracy of < 1 cm. The system used plastic frames with reflective markers on which the TSA antennas were also mounted to obtain UWB and VICON motion capture data simultaneously. Measurements in the frequency domain were performed in the UWB range (3-10 GHz) using a 4-port vector network analyzer. For each on-body sensor location (mobile station (MS)) and BS link, S_{21} parameters data was collected from the VNA with a sweep of 6400 data samples.

A. L-shape Localization

The compact L-Shape configuration (Fig. 1 (b)) requires only 3 BSs to achieve accurate 3D localisation [17]. First TOA data fusion method is used to obtain the estimated values for the x_m and z_m coordinate of the target. To obtain the third coordinate y_m, the following equations are used:

$$\theta = \cos^{-1}\frac{z_m}{R\_est} \tag{1}$$

$$S = \frac{z_m}{\tan(90-\theta)} \tag{2}$$

$$y_m = \sqrt{S^2 - x_m^{\,2}} \tag{3}$$

where *R_est* is the estimated distance from the BS1 (origin) to the target P. θ is the zenith angle and S is the projected distance of point P from origin in the *x-y* plane.

Four variations of the L-Shape BS configuration are analyzed namely: (L1, L2, L3 and L4) positioned in the *x-z plane* and *y-z plane* as shown in Fig. 2. BS1,2_A and BS1,2_B are common BSs positions for Fig. 2 (a)-(b) and Fig. 2 (c)-(d) respectively. BS3 is denoted as $BS3_{c1}$/$BS3_{c2}$ and its location can be in the *x-z*/*y-z plane* depending on the orientation in which the L-Shape configuration is positioned.

B. Localization Algorithm

The localisation algorithm is designed to take into account the NLOS and MPCs effects and mitigating positive bias error to obtain high accuracy body-centric localisation. The algorithm uses off-body channel information and TOA peak detection and data fusion techniques [3].

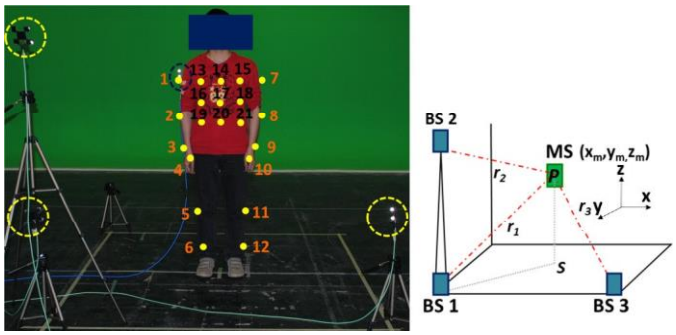

(a) (b)

Fig. 1. (a) Experiment set up: *x-z plane* L-Shape base station configuration and human subject present in the center of the localisation area with the wearable sensor mounted on the right shoulder. (b) L-Shape base station configuration schematic.

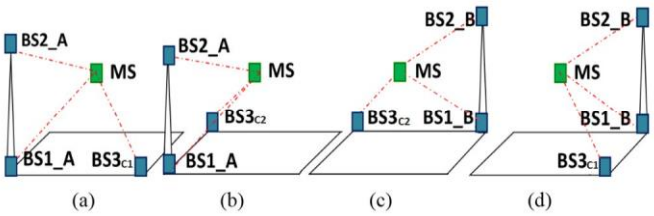

Fig. 2 L-Shape base station configurations: (a) L1: x-z plane, facing forward (b) L2:y-z plane, facing side right (c) L3: x-z plane, facing backward (d) L4: y-z plane, facing side left.

Firstly, the channel impulse response (CIR) is computed by applying Inverse Fast Fourier Transform (IFFT) to the measured S_{21} parameters obtained for each MS-BS links. The total line of sight (LOS) situations are distinguished from the NLOS/partial (P) NLOS links which suffer high attenuation by using the peak signal strength of the power delay profile (PDP) as indicator. Fine classification of the NLOS and PNLOS/PLOS links is carried out by analyzing two channel parameters: RMS delay spread (σ_τ) and Kurtosis (κ) . σ_τ [1819] describes the time dispersive properties of the channel is defined as:

$$\sigma_\tau = \sqrt{\frac{\Sigma_k (\tau_k - \tau_m)^2 \cdot |h(\tau_k; d)|^2}{\Sigma_k |h(\tau_k; d)|^2}} \qquad (4)$$

where τ_k are the multipath delays relative to the first arriving multipath component and d is the separating distance between the Tx and Rx. The Kurtosis is a statistical parameter that indicates the fourth order moment of the received signal amplitude [3,17-18]. κ is mathematically defined as follows:

$$\kappa(x) = \frac{1}{\sigma^4} \frac{\Sigma i (x_i - \bar{x})^4}{N} \qquad (5)$$

where σ is the standard deviation of the variable x and $\bar{x}$ is the mean value of x. N is the number of samples. σ_τ / κ is higher/lower for NLOS links in comparison to LOS links due to the high MPCs and spread of the channel.

For line-of-sight (LOS) links, estimated TOA of the UWB signal between the target and BS is computed using maximum peak detection algorithms [3, 20]. Threshold based leading edge detection algorithms are considered for obtaining accurate range/TOA estimate for total NLOS links between the wearable sensors and BSs [3,20]. The estimated range (r) information is applied in the localisation algorithm which uses trilateration and least square solution approach to estimate the unknown position *(! , ,;)* of the on-body sensors which are located on the human subject [22].

$$r_i^2 = (x_i - x_m)^2 + (y_i - y_m)^2 + (z_i - z_m)^2 \qquad (6)$$

where i =1,2,3,4 and r_i represents the computed range between the MS and BS obtained from the channel data.

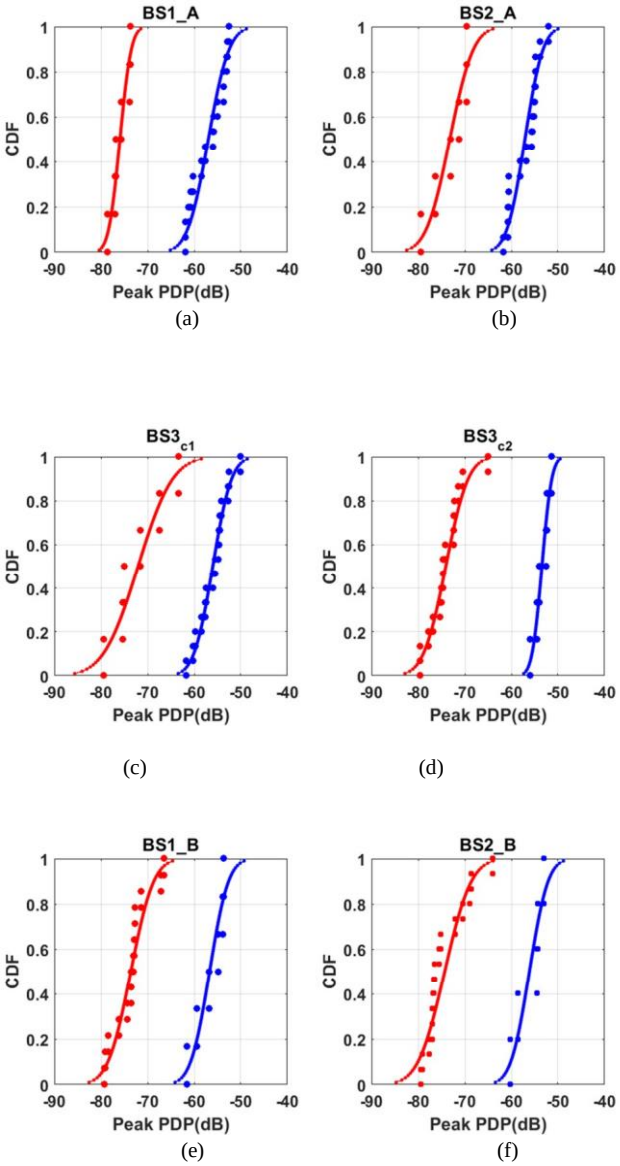

Fig. 3. Cumulative distribution function for the peak power delay profile for various locations of the wearable sensors and base stations ((a) BS1_A, (b) BS2_A, (c) $BS3_{c1}$ and (d) $BS3_{c2}$ (e) BS1_B (f) BS2_B). Coarse classification of the LOS (blue) and NLOS (red) links for each Tx-Rx pair.

III. Results and Analysis

In order to distinguish between total LOS and NLOS scenarios, peak value of the PDP is detected. Figure 3 (a)-(f) depicts the classification (LOS or NLOS) of the peak PDP for various on-body antenna locations with respect to each BS position. From the graph Fig 3 (a)-(f), it can be seen that BS1,2_A and $BS3_{c1}$ have high occurrence of lower magnitude of attenuation (-65 to -50 dB). BS1,2_A form LOS/PLOS links with the right limbs (S1-S6) and the torso region (S13-S21) of the human subject. $BS3_{c1}$ forms LOS links with the sensors placed on the left limbs (S7-S12) and torso region. BS1,2_B, $BS3_{c2}$ has higher occurrence of attenuation (-80 to -65 dB) depicting total/partially obstructed path. The human subject is facing back, hence, the links formed are NLOS (left or right limbs) and torso region leading to higher attenuation of the received signal. Peak magnitude of the PDP can aid in distinguishing between total LOS from other channel types such as PNLOS and NLOS links, peak PDP normally in the range of -65 to -50 dB represents total LOS links and -80 to -65 dB indicates presence of NLOS links.

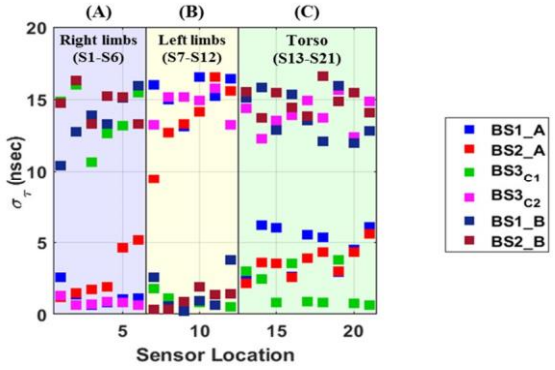

Fig. 4. RMS delay spread for various locations of the wearable sensors for each of the base stations position (BS1,2_A, BS3$_{c1}$, BS3$_{c2}$ and BS1,2_B). OnBody sensor positions: (a) Right limbs (S1-S6) (b) Left limbs (S7-S12) (c) Torso (S13-S21).

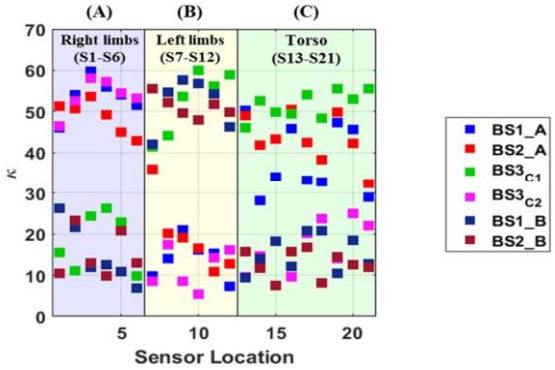

Fig. 5. Kurtosis for various locations of the wearable sensor for each of the base stations positions (BS1,2_A, BS3$_{c1}$, BS3$_{c2}$ and BS1,2_B). On-Body sensor positions: (a) Right limbs (S1-S6) (b) Left limbs (S7-S12) (c) Torso (S13-S21).

σ_τ and κ for various off-body links with respect to different BSs positions is presented in Fig. 4 (a)-(c) and Fig. 5 (a)-(c).

As observed in Fig. 4 (a) and Fig. 5 (a), σ_τ /κ range from (0.5-5 nsec)/(40-60) for BS1,2_A and BS3$_{c2}$ indicating LOS links between the BSs and the wearable sensor. NLOS links indicate high multipath and with the values ranging from 1016 nsec for For BS1,2_B, BS3$_{c1}$, the wearable sensors on the right limbs form NLOS links which is due to the location of the wearable sensors leading to obstructed path. & for NLOS are lowest with values ranging from 5-25.

The channel parameter values for the sensors placed on the left limbs (S7-S12) are given in Fig. 4 (b) and Fig. 5 (b). For the case of the left limbs, LOS scenario is observed for BS1,2_B and BS3$_{c1}$ due to the direct path between the wearable sensors and BS. The values of σ_τ and κ are in the range of (0.5-4 nsec) and (40-60) respectively. For the BS1,2_A and BS3$_{c2}$, the left limb exhibits NLOS and PNLOS links which can be seen by the values obtained for the channel parameters presented in Fig. 4 (b) and Fig. 5 (b). κ in the range of 10-35 is observed, with 10-25 indicating total NLOS and values between 25-40 indicating PNLOS scenarios. σ_τ of 10-20 nsec indicate NLOS links and between 6-10 nsec represent PNLOS links.

The torso region depicts variable link types ranging from LOS, PLOS/PNLOS and NLOS scenarios which can be observed in Fig. 4 (c) and Fig. 5 (c) channel parameter values. LOS and PLOS links are observed for σ_τ and κ in the range of 0.5-6 nsec and 30-60 for BS1,2_A off-body links. For BS3$_{c1}$ generally LOS links are observed with values ranging 0.5-5 nsec and 45-55 for σ_τ and κ respectively. For BS1,2_B, BS3$_{c2}$ total NLOS scenarios occur as the human subject is acting as an obstruction between the BS and the wearable sensors placed on the torso. σ_τ varies between 12-16 nsec and κ in the range of 10-25 indicating high multipath components and spread of the received signal, leading to decrease in signal strength and distortion.

TABLE I. CHANNEL CLASSIFICATION FOR L-SHAPE BS CONFIGURATIONS

Wearable sensor Location	BS1_A	BS2_A	$BS3_{c1}$	$BS3_{c2}$	BS1_B	BS2_B
Right Limbs S1-S6	LOS	LOS	NLOS PNLOS	LOS	NLOS PNLOS	NLOS PNLOS
Left Limbs S7-S12	NLOS PNLOS	NLOS PNLOS	LOS	NLOS	LOS	LOS
Torso S13-S19	LOS PLOS	LOS PLOS	LOS	NLOS	NLOS	NLOS

Table I presents the classification of the type of body centric links formed between the different BSs of the four LShape configurations and location of the body-worn sensor. L1: BS1,2_A and $BS3_{c1}$; L2: BS1,2_A and $BS3_{c2}$; L3: BS1,2_B and $BS3_{c2}$; L4: BS1,2_B and $BS3_{c1}$ comprises the four L-Shape configurations analyzed. L1 has higher number of LOS links (70 %) in comparison to L2 (57 %), L3 (30 %), L4 (42 %). Hence, the NLOS mitigation techniques have to be only applied on less number of the wearable sensor-BS links in order to obtain high accuracy results and also reducing computational time. The plane (*x*-*z* or *y*-*z*) in which the LShape configuration is placed, significantly influences the channel type formed with minimum NLOS for L1 and maximum for L3 L-shape configuration.

High accuracy body-centric localisation is obtained using channel information, TOA data fusion algorithms and compact L-Shape configurations. The average error obtained for L1, LShape configuration (Fig. 6 (a), torso region) is in the range of 1-3 cm and L3, L-Shape configuration (Fig. 6 (b), torso region) localisation accuracy is in the range of 2-4 cm. The difference in accuracy between the L-Shape BS configurations is due to the fact that L3 has 2.5 times higher occurrence of NLOS links leading to some deterioration in range estimation and further affecting the localisation accuracy.

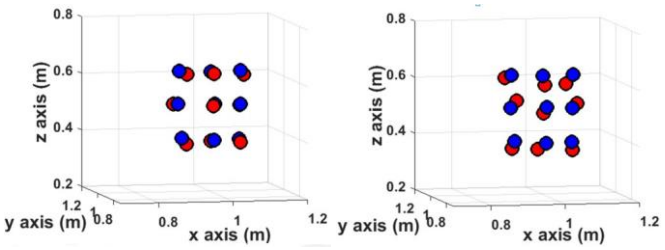

(a) (b)

Fig. 6. 3D localisation of the torso region on-body nodes using IR-UWB (red) and VICON motion capture system as reference (blue) L-Shape configuration (a) L1 (b) L3.

A comparison of various state-of-art UWB localization techniques has been provided in Table II. Integrated UWB and inertial technology provides a human localization accuracy of < 13 cm [13], indoor motion gaming tracks the arm motion by LOS/obstructed (O) LOS: 2-11/7.5-24 cm [11], indoor localization applying extended finite impulse response (EFIR) estimator provides 20-50 cm accuracy [12] and tracking sports person by UWB tags reported a ranging accuracy of 22 cm [10]. The L-shape configuration has achieved substantial increase in 3D body-centric localization accuracy by using a compact 2D plane BSs placement and channel information when compared to the available methodologies reported. The L-Shape configuration is a good trade-off between the number of BSs needed, volume occupancy of the BSs and accuracy.

TABLE II. STATE-OF-ART UWB POSITIONING TECHNIQUES

Ref.	UWB System/Technique	BSs	Accuracy (cm)
[8]	UWB transreceiver/MEMS sensors; TDOA	5 3D	1 m (90 %)
[9]	UWB ray tracing algorithm; TOA/TWR	16 3D	LOS & NLOS mixed x-y/z 25/1 cm
[10]	UWB transreceiver; TOA/TDOA	8 3D	Ranging: 22 cm
[11]	UWB antennas/VNA; TOA/RSS	2 1D	LOS/OLOS 2-11/7.5-24 cm
[12]	UWB transreceiver; TOA	4 3D	20-50 cm
[13]	IMU/UWB Tags; AOA/TDOA	4 3D	< 13 cm
[15]	Geometrical properties of propagation paths	1 2D	LOS/OLOS/NLOS 26/28/90 cm
[16]	UWB equilateral triangular array antenna Rx center; TDOA	3 2D	5 cm

IV. CONCLUSION

This work successfully demonstrates the use of compact 2D plane L-Shape BS configuration using channel information and time of arrival range estimation techniques, without compromising the accuracy of 3D localisation. NLOS channel parameters values in the range of (Peak PDP, τ_{rms}) is high by (15-20 dB, 10-15 nsec) and & is low by 20-30 when compared with the average values obtained for LOS links. The four orientations of the L-Shape configuration provide high accuracy in cm range with the *x-z plane* configuration facing front providing higher accuracy (1-3 cm) due to the maximum occurrence of direct paths. The impact of the channel parameters has significant role to play in the UWB system performance and position estimation. The work presented can be used for several UWB-BAN applications and evaluating body-centric multipath propagation in indoor environments.

REFERENCES

[1] R. Cavallari, F. Martelli, R. Rosini, C. Buratti and R. Verdone, "A Survey on Wireless Body Area Networks: Technologies and Design Challenges," in *IEEE Commun. Surveys & Tutorials*, vol. 16, no. 3, pp. 1635-1657, Third Quarter 2014.

[2] M. R. Mahfouz, A. E. Fathy, M. J. Kuhn and Y. Wang, "Recent trends and advances in UWB positioning," *2009 IEEE MTT-S Int. Microwave Workshop on Wireless Sensing, Local Positioning, and RFID*, Cavtat, 2009, pp. 1-4.

[3] R. Bharadwaj, S. Swaisaenyakorn, C. G. Parini, J. C. Batchelor and A. Alomainy, "Impulse Radio Ultra-Wideband Communications for Localization and Tracking of Human Body and Limbs Movement for Healthcare Applications," in *IEEE Trans. on Antennas and Propag.*, vol. 65, no. 12, pp. 7298-7309, Dec. 2017.

[4] A. Alomainy, A. Sani, A. Rahman, J. G. Santas and Y. Hao, "Transient Characteristics of Wearable Antennas and Radio Propagation Channels for Ultrawideband Body-Centric Wireless Communications," in *IEEE Trans. Antennas Propag.*, vol. 57, no. 4, pp. 875-884, April 2009.

[5] G. Oguntala G., R. Abd-Alhameed R., S. Jones S., J. Noras, M. Patwary, J. Rodriguez, "Indoor location identification technologies for real-time IoT-based applications: An inclusive survey", *Computer Science Review*, Vol. 30,2018, Pages 55-79.

[6] H. A. Shaban, M. A. El-Nasr and R. M. Buehrer, "Toward a Highly Accurate Ambulatory System for Clinical Gait Analysis via UWB Radios," in *IEEE Trans. on Information Technol. in Biomedicine*, vol. 14, no. 2, pp. 284-291, March 2010.

[7] H.T. Dinh., C.L. Law and R.C.L. Wei, "3-D localisation system using 4 anchors employing ultra-wideband impulse radio," *2015 10th Int. Conf. on Information, Commun. and Signal Processing (ICICS)*, Singapore, 2015, pp. 1-5.

[8] V. Djaja-Josko and J. Kolakowski, "UWB positioning system for elderly persons monitoring" *2015 23rd Telecommunications Forum Telfor (TELFOR)*, Belgrade, 2015, pp. 169-172.

[9] J. Hyun, T. Oh, H. Lim and H. Myung, "UWB-based Indoor Localization Using Ray-tracing Algorithm," *2019 16th International Conference on Ubiquitous Robots (UR)*, Jeju, Korea (South), 2019, pp. 98-101.

[10] Minne, K.; Macoir, N.; Rossey, J.; Van den Brande, Q.; Lemey, S.; Hoebeke, J.; De Poorter, E. Experimental Evaluation of UWB Indoor Positioning for Indoor Track Cycling. *Sensors* 2019, *19*, 2041.

[11] Y. Zheng, Y. Zang and K. Pahlavan, "UWB localization modeling for electronic gaming," *2016 IEEE International Conference on Consumer Electronics (ICCE)*, Las Vegas, NV, 2016, pp. 170-173.

[12] Y. Xu, Y. S. Shmaliy, Y. Li, X. Chen, "UWB-based indoor human localization with time-delayed data using EFIR filtering", *IEEE Access*, vol. 5, pp. 16676-16683, 2017

[13] P. K. Yoon, S. Zihajehzadeh, B. Kang and E. J. Park, "Robust Biomechanical Model-Based 3-D Indoor Localization and Tracking Method Using UWB and IMU," in *IEEE Sensors Journal*, vol. 17, no. 4, pp. 1084-1096, 15 Feb.15, 2017.

[14] R. Bharadwaj, A. Alomainy and C.G. Parini, "Experimental Investigation of 3D Human Body Localisation Using Wearable Ultra Wideband Antennas," *IEEE Trans. on Antennas and Propag.*, vol.63, no.11, pp.5035-5044, Nov. 2015.

[15] Hanssens *et al*., "An Indoor Variance-Based Localization Technique Utilizing the UWB Estimation of Geometrical Propagation Parameters," in *IEEE Transactions on Antennas and Propagation*, vol. 66, no. 5, pp. 2522-2533, May 2018.

[16] M. Li *et al*., "Localization of an UWB Mobile Station with Sparse Antenna Array and Reference Station," *2018 IEEE International Conference on Computational Electromagnetics (ICCEM)*, Chengdu, 2018, pp. 1-3.
[17] R. Bharadwaj, C.G. Parini and A. Alomainy, "Ultrawideband-Based 3-D Localization Using Compact Base-Station Configurations," in *IEEE Antennas Wireless Propag. Lett.*, vol. 13, pp. 221-224, 2014.
[18] R. Bharadwaj, S. Swaisaenyakorn, J. C. Batchelor, S. K. Koul and A. Alomainy, "Base-Station Random Placement Effect on the Accuracy of Ultrawideband Body-Centric Localization Applications," in *IEEE Antennas Wireless Propag. Lett.*, vol. 17, no. 7, pp. 1319-1323, July 2018.
[19] T.S. Rappaport T.S., Wireless Communications Principles and Practice. Prentice Hall, Inc., New Jersey, 1996.
[20] Guvenc I., Chong C.C., "A Survey on TOA Based Wireless Localization and NLOS Mitigation Techniques," *IEEE Commun. Surveys & Tuts.*, vol.11, no.3, pp.107-124, 3rd Quarter 2009.
[21] S. Marano, W. M. Gifford, H. Wymeersch and M. Z. Win, "NLOS identification and mitigation for localization based on UWB experimental data," in *IEEE J. on Selected Areas in Commun.*, vol. 28, no. 7, pp. 1026-1035, September 2010.
[22] Y. Lee, D. Kang, K. Moon and S. Cho, "Enhancement of the real-time indoor ranging and positioning algorithm using an UWB system," *2017 IEEE 17th Int. Conf. on Ubiquitous Wireless Broadband (ICUWB)*, Salamanca, 2017, pp. 1-4.